Mott breakdown effect in spinel $MgTi_{1.2}V_{0.8}O_4$

A. Rahaman,[1,2] T. Paramanik,[1,3] R. K. Maurya,[4] K. Yadav,[4] R. Bindu,[4] K. Mukherjee,[4] and D. Choudhury[1,*]

[1]*Department of Physics, Indian Institute of Technology Kharagpur, Kharagpur 721302, India*

[2]*Department of Physics, Yogoda Satsanga Palpara Mahavidyalaya, Palpara- 721458, India*

[3]*Department of Physics, School of Sciences, National Institute of Technology Andhra Pradesh, Tadepalligudem 534102, India*

[4]*School of Basic Sciences, Indian Institute of Technology Mandi-Kamand, Himachal Pradesh 175005, India*

(Received 27 March 2020; revised 23 May 2021; accepted 17 June 2021; published 28 June 2021)

Materials in which a Mott insulator to metal transition (Mott breakdown) can be induced using a moderate dc current (with an electric field that is much smaller than the corresponding Zener breakdown voltage) is extremely promising for electronic device applications and offer a unique platform for investigation of the underlying emergent mechanism. Here we report a Mott breakdown phenomenon in a spinel compound, namely, $MgTi_{1.2}V_{0.8}O_4$, which undergoes a sharp switching of resistivity by several orders of magnitude by application of a dc current. The observed Mott breakdown effect, which is associated with a negative differential resistance as seen in the corresponding electric-voltage (V) vs electric-current (I) curve (opposite to Ohm's law dependence), occurs beyond a temperature-dependent threshold electric current (I_{th}), which corresponds to an extremely small threshold electric-field (E_{th}) (for example, E_{th} is found to be ~40 V/cm at 50 K and further decreases with an increase in temperature). The system remains in the metastable metallic state only in the presence of high-current flow upto the lowest measured temperature and switches back to the highly insulating state when the current flow is switched off. Associated experimental observations suggest against a Joule-heating driven change in state and hint towards an electronic mechanism. Using first-principles calculation and several experimental probes, we further investigate the origin of the driving mechanism. The presence of two Jahn-Teller active ions, i.e., Ti^{3+} ($3d^1$—one electron among three t_{2g} levels) and V^{3+} ($3d^2$—two electrons among three t_{2g} levels) in $MgTi_{1.2}V_{0.8}O_4$ along with the obtained density of states offers a unique opportunity which seems critical for the Mott breakdown phenomenon as it supports high-current induced excitation of electrons through an activated avalanche process from Ti^{3+} t_{2g} levels (located at the edge of the valence band) into V^{3+} t_{2g} levels (located at the bottom of the conduction band) thereby removing the orbital degrees of freedom of the V and Ti electrons and leading to melting of the Jahn-Teller driven structural transition into the insulating tetragonal phase.

DOI: 10.1103/PhysRevB.103.245145

Strongly correlated electron systems exhibit a plethora of functional properties [1–8], including metal-to-insulator transition [9–11], and serve as a cradle for multiple emergent physics. In Mott insulators, due to strong Coulomb repulsion, electrons remain localized on atomiclike orbitals, which, thus, remain unavailable for electrical conduction process. Excitingly, breaking of the many-body Mott-insulating state to make the charge carriers free for electrical conduction have been demonstrated by adopting several techniques, such as photoexcitation [12], through charge-carrier doping, and by applying hydrostatic pressure [9]. Among such techniques, application of electric pulse or passing electric current to induce breakdown of the Mott-insulating phase is of immense interest and being actively investigated due to its application in electronic devices. The promising realization of the emergent metallic state by collapsing the insulating Mott gap with a low electric field or current (much smaller than the Zener breakdown limit) is extremely challenging and have been limited to only few selected systems [13–19]. However, in such cases, elucidation of the microscopic mechanisms that lead to such a novel phenomenon largely remains an open problem. In this paper, we report the breakdown of an insulating state in a spinel system, namely, $MgTi_{1.2}V_{0.8}O_4$ (MgTVO) (which is a solid-solution member of two insulating spinel oxides, $MgTi_2O_4$ and MgV_2O_4) in the presence of dc current flow corresponding to a record low E_{th}. Although MgTVO remains in the highly insulating state throughout the temperature range in the presence of a small dc current, a sharp drop in resistivity by several orders of magnitude (measured in linear four-probe geometry) from the insulating to a metallic state is observed on application of a moderate dc current ($I > I_{th}$). One of the parent spinels of MgTVO, namely, $MgTi_2O_4$, contains orbitally active Ti^{3+} ions and undergoes a cooperative Jahn-Teller (JT) effect driven structural transition (accompanied with a spin-singlet transition) from a cubic Fd-$3m$ to a chiral tetragonal $P4_12_12$ structure at 260 K [20–24]. The other parent member, MgV_2O_4 also comprises orbitally active V^{3+} ions and undergoes a JT-effect driven structural transition from cubic Fd-$3m$ to tetragonal $I4_1/a$ at 62 K followed by a lower-temperature antiferromagnetic ordering at 40 K [25]. Curiously, the ground-state structure of the solid-solution compound MgTVO is found to contain both kinds of ions, i.e., orbitally inactive Ti^{4+} ($3d^0$) and V^{2+} ($3d^3$)

*debraj@phy.iitkgp.ac.in

ions (due to energetically favorable transfer of a 3*d* electron from a Ti^{3+} ion to a V^{3+} ion) along with the presence of orbitally active Ti^{3+} and V^{3+} ions (the copresence of orbitally active V^{3+} ions is found necessary to optimize the lattice strain energy, which comes accompanied with the much larger V^{2+} ions). The partial density of states (DOS) of MgTVO sheds light on the possible mechanism of the observed Mott breakdown effect, which likely proceeds with current-induced excitations of electron (through an avalanche process) across the band gap from Ti^{3+} into V^{3+} levels thereby melting the JT-effect driven structural transition. Since such a field-induced metastable metallic state and the insulating state have very different orbital polarizations (arising from varying orbital degrees of freedom), a small threshold field for metallization can, therefore, be expected as shown using model calculations [26].

Polycrystalline samples of MgTVO were prepared using the solid-state reaction method by mixing MgO, TiO_2, V_2O_3, and Ti powders and annealing at 1080 °C in a vacuum sealed quartz tube. X-ray diffraction (XRD) and Rietveld refinement [27] were used to investigate the phase formation and lattice parameters of the sample. Temperature-dependent linear four-probe resistivity, heat-capacity, and dielectric constant measurements were performed using the physical property measurement system (Cryogenic Limited, U.K.) and a closed-cycle cryostat, respectively. The ohmic nature of the electrical contacts (possessing small contact resistance values), used for the four-probe resistivity measurements, were verified [28–30]. To investigate the magnetic properties and valence state of the system, we have used the magnetic property measurement system and x-ray photoelectron spectroscopy (XPS), respectively. All XPS spectra were corrected for any charging effects by using the C 1*s* binding-energy position as a reference. The electronic structure calculations were performed using density functional theory by considering a plane-wave basis as implemented in the Vienna *ab initio* simulation package [31]. The generalized gradient approximation (GGA) for the exchange-correlation functional along with electron-electron correlation (GGA + U) [32] were considered with 37.5% V ions doped at the Ti site (six V and ten Ti ions in a cubic unit cell, close to the 40% experimental doping percentage) in $MgTi_2O_4$. We have taken the experimental lattice parameters of MgTVO and performed GGA + U calculations with internal geometry optimizations using various magnetic configurations [nonmagnetic, ferromagnetic (FM), antiferromagnetic (AFM)]. For reciprocal space integrations, we have used 6 × 6 × 6 Γ-centered k mesh and have adopted a plane-wave cutoff of 500 eV.

The temperature dependencies of four-probe resistivity of MgTVO, measured in both heating and cooling cycles with constant current (I) values of 0.1 and 100 mA are shown in Fig. 1(a). For a constant-current measurement with 0.1 mA, the sample remains in the insulating state throughout the temperature range in both heating and cooling cycles. In sharp contrast, an extremely sharp drop in resistivity is observed in the heating run around 45 K from a large resistivity value (beyond the measurement limit of our setup) to 0.2 Ω cm for 100-mA current. Interestingly, in the cooling run with 100-mA current, the sample continues to remain in the metallic phase even below 45 K (the small positive temperature

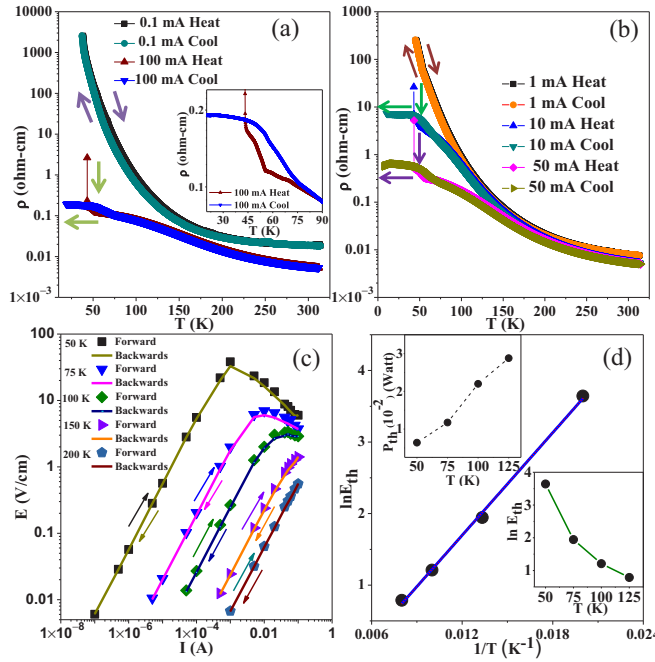

FIG. 1. Temperature dependencies of resistivity, measured with (a) 0.1- and 100-mA currents and with (b) 1-, 10-, and 50-mA currents in both heating and cooling cycles. The inset to (a) shows low-temperature resistivity hysteresis. (c) Current dependencies of electric-field values in both forward and backward current sweeps exhibiting negative differential resistance beyond a temperature-dependent threshold electric-field (E_{th}) value. (d) shows the linear dependence of $\ln(E_{th})$ on $1/T$ [the lower inset shows $\ln(E_{th})$ does not depend linearly on temperature]. The upper inset shows an increase in threshold power (P_{th}) with the sample base temperature.

coefficient of resistivity is likely from grain-boundary effects [33–35]). In all isocurrent measurements where we observe a sharp drop in resistivity values in the heating run, a metastable metallic state is realized until the lowest temperatures in the cooling run. Importantly, the current-induced metallization in MgTVO is found to exhibit many characteristic features as discussed below, which are incompatible with Joule heating as the driving mechanism [28,36–40]. As shown in the upper inset of Fig. 1(d), the threshold power to induce the high-resistance state to the low-resistance state transition at a given temperature is found to increase with the increase in the sample base temperature [36,40]. Clearly, in the event that the resistivity state transition is induced by the Joule-heating mechanism, the threshold power to induce the resistivity state transition is known to decrease with the increase in sample base temperature [36,40,41]. Furthermore, as seen in Fig. S4 of the Supplemental Material [28], the sharp drop in resistivity values in the heating run from the high-resistance to the low-resistance state occurs at the same temperature for various applied currents. When such an effect is driven by Joule heating, the drop in resistivity values is expected to occur at a higher temperature for a lower applied current, which is clearly inconsistent with the present experimental observations. Also, the clear absence of any hysteresis in the various isothermal E-I curves [as seen in Fig. 1(c)] between the increasing and the decreasing current sweep curves across

the threshold current suggest against Joule heating [42,43] or any irreversible chemical change to be the driving force behind the observed resistive state transition in MgTVO.

The breakdown of the insulating state also gets reflected in the isothermal voltage(V)-I curves where after a certain threshold electric-field ($E_{\rm th}$), the V-I curve deviates from an Ohm's law dependency (positive linear $\frac{\Delta V}{\Delta I}$), and a negative $\frac{\Delta V}{\Delta I}$ is obtained thereby leading to a negative differential resistance (NDR). Similar NDR effects have been observed in other systems where a breakdown of the corresponding insulating state can be triggered through an applied electric field [13–15,44]. Excitingly, $E_{\rm th}$ for MgTVO is extremely small even at low temperatures, for example, $E_{\rm th} = 38$ V/cm at $T = 50$ K. Furthermore, $E_{\rm th}$ for MgTVO is found to decrease with increasing temperature as seen in Fig. 1(c) (E-I curves for some other temperatures are shown in Fig. S5 of the Supplemental Material [28]). A clear linear and direct dependence is observed for the obtained (ln $E_{\rm th}$) values against $\frac{1}{T}$ as seen in Fig. 1(d), suggesting thermally activated [16,17,45] dependency $\frac{E_{\rm th}(T)}{E_{\rm th}(0)} = \exp(\frac{\Delta}{KT})$.

The abruptly sharp transition in resistivity data (for example, in the heating run with 100-mA current) along with the presence of hysteresis in resistivity values obtained between the heating and the cooling runs [shown in the inset of Fig. 1(a)], suggests the presence of a low-temperature first-order transition. We next discuss the magnetic properties to investigate any magnetic origin to such a transition. The temperature-dependent magnetic susceptibility (χ) of MgTVO as shown in Fig. 2(a), exhibits no magnetic anomaly in the entire temperature range between 10 and 300 K. A modified Curie-Weiss law [$\chi = C/(T-\theta)+\chi_0$] [46] with a small negative Curie-Weiss temperature of ~ -4 K (suggesting AFM spin interactions), can nicely explain the magnetic data below 200 K. Two magnetic transitions are clearly discernible from the derivative magnetization ($\frac{d\chi}{dT}$) data, the first transition observed around 5 K [shown in the upper inset of Fig. 2(a)]. This, along with extracted negative Curie-Weiss temperature, indicates an antiferromagnetic ordering at 5 K in MgTVO. The second, and much weaker transition, seen in $\frac{d\chi}{dT}$ around 338 K, is also associated with a distinct small drop in magnetization value [shown in the lower inset to Fig. 2(a)] and is indicative of a much-weakened spin-singlet transition than the parent spinel $MgTi_2O_4$ [20]. The resistivity values (for both the heating and the cooling runs along with the sharpness of resistivity transition in the heating run) remain similar when measured either in the presence or in the absence of a 7-T magnetic field (Fig. S7 of the Supplemental Material [28]). All above observations clearly rule out any magnetic origin to the low-temperature first-order transition.

To investigate a possible structural origin of the first-order transition, we discuss the temperature dependencies of the dielectric-constant data. A low-temperature transition is clearly discernible as a sharp dip in the dielectric constant ($\epsilon_{\rm r}$) data (the transition temperature of the dip remains same for various applied frequencies, which is suggestive of a first-order transition) as shown in Fig. 2(b). Around similar temperature, a clear transition is also seen in the corresponding heat-capacity (C) data as seen in the $\frac{C}{T}$ vs T data [shown in the inset of Fig. 2(b)]. To investigate the

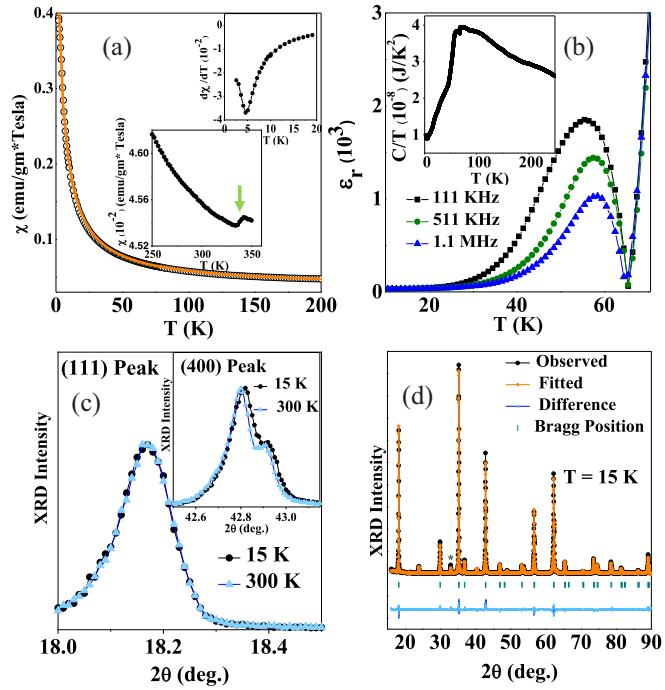

FIG. 2. (a) Curie-Weiss fitting of the magnetic susceptibility (χ) data measured with 0.1 T. The magnetic transition is discernible at 5 K as seen from $\frac{d\chi}{dT}$ data (upper inset). A drop in susceptibility (χ) is also observed around 338 K (lower inset). (b) Temperature (T) dependent dielectric constant (ϵ_r) values exhibiting a frequency dispersionless transition around 65 K. The inset shows specific-heat (C) also exhibits a low-temperature transition as seen in $\frac{C}{T}$ vs$T$ data. (c) The (111)-XRD peak exhibits no temperature-dependent broadening, whereas, broadening is observed for the (400)-XRD peak at low temperature as compared to room temperature (shown in the inset). (d) Rietveld refinement of the 15-K XRD spectrum with the tetragonal $I4_1/a$ structure along with the nonconducting diamagnetic impurity phase of $MgTiO_3$ (∼4%, indicated with an asterisk).

origin of the low-temperature transition, we have performed XRD investigations both above (300 K) and below (15 K) the phase transition. The (111)-XRD-peak, observed at both temperatures, overlaps on each other [Fig. 2(c)] and does not show any additional temperature-dependent broadenings. However, the (400)-XRD peak shows additional broadening at 15 K compared to the 300-K spectra [as seen in the inset of Fig. 2(c), the (311)- and (440)-XRD peaks also show similar low-temperature broadenings as shown in Fig. S8 of the Supplemental Material [28]). Such low-temperature broadenings only in selective XRD peaks, although notably opposite to the usual thermal-broadening effect, is consistent with a higher-temperature cubic to lower-temperature tetragonal structural transition. Similar observations on related spinel oxide $MnTi_2O_4$, have been used as a characteristic tool to detect weak (with the pseudocubic lattice parameters being closely similar in the tetragonal phase) structural transitions [48,49]. In consistence with this scenario, the 15-K XRD spectrum of MgTVO could be fit [Fig. 2(d)] better with a tetragonal $I4_1/a$ structure (ground-state space group of MgV_2O_4) rather than the cubic Fd-$3m$ space group or the tetragonal $P4_12_12$ space group (ground state of $MgTi_2O_4$).

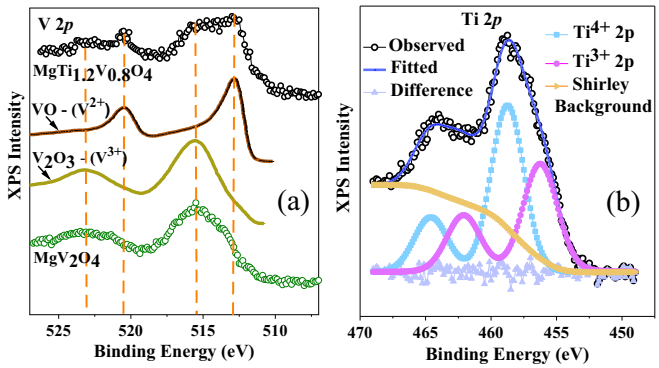

FIG. 3. (a) Comparison of the V $2p$ XPS spectra of $MgTi_{1.2}V_{0.8}O_4$ with reference spectra for the V^{3+} ion (V_2O_3 [47] and MgV_2O_4) and the V^{2+} ion (VO [47]). (b) Deconvolution of the Ti $2p$ XPS spectra into contributions from Ti^{3+} and Ti^{4+} ions.

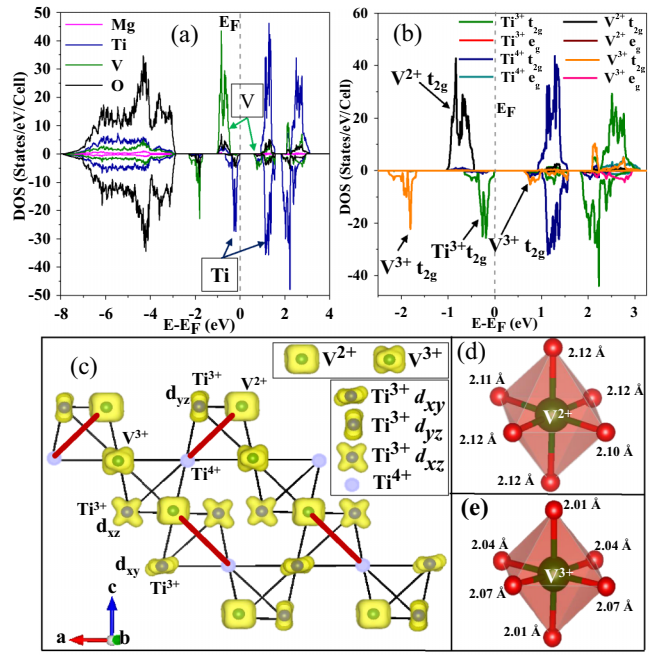

FIG. 4. Spin-resolved total density of states for various atoms in (a) and (b) shows the corresponding e_g and t_{2g} levels of the constituent ions. (c) shows the charge-density plot of the distorted cubic phase. Thick red lines indicate bonds involving charge transfer from Ti to V ions. (d) and (e) show the corresponding VO_6 octahedra involving V^{2+} and V^{3+} ions.

Having elucidated a structural origin to the observed first-order transition in MgTVO, we next discuss the valence states of its constituent V and Ti ions since they affect the transport properties significantly. Interestingly, the V $2p$ and Ti $2p$ XPS spectra of MgTVO, recorded at room temperature [as shown in Figs. 3(a) and 3(b) and the O $1s$ spectrum shown in Fig. S9 of the Supplemental Material [28]), clearly elucidate the mixed-valence states for both V and Ti ions, i.e., MgTVO contains orbitally inactive V^{2+} ($3d^3$) and Ti^{4+} ($3d^0$) ions along with the presence of orbitally V^{3+} ($3d^2$) and Ti^{3+} ($3d^1$) ions. Such diluted presence of JT-active ions (V^{3+} and Ti^{3+} ions) in MgTVO as compared to its parent spinels, $MgTi_2O_4$ (only Ti^{3+} ions) and MgV_2O_4 (only V^{3+} ions), clearly elucidate the weakening of JT driven structural transition in MgTVO. Similar mixed valence states for V and Ti ions are also inferred from the first-principles calculations on V-doped $MgTi_2O_4$ (Fig. S10 of the Supplemental Material [28]). Since a current-induced metallic phase is realized in MgTVO over the temperature window from 50 K to around 200 K [as shown in Fig. 1(c) and Fig. S6 of the Supplemental Material [28]), we discuss next the electronic structure of the high-temperature distorted cubic phase of MgTVO. Figure 4(a) shows the DOS of the distorted Fd-$3m$ structure of V-doped $MgTi_2O_4$, obtained with U values of (3,4) eV for (Ti,V) (similar U values were used in related systems [22,50]), which gives an insulating character in consistence with experiments. We focus here on the relative position of the orbitals positioned across the band gap, which remains invariant for either the FM or the AFM spin orderings as illustrated in Fig. S11 of the Supplemental Material [28]. Among the many Ti^{3+} ions with which the doped V (V^{3+}) ion share edges in the corner-sharing tetrahedral geometry of the spinel structure, a complete transfer of an electron is observed to occur from a single Ti ion to the V ion [shown in Fig. 4(c)]. Since the resultant V^{2+} ion from such a process has a much larger ionic radii (0.79 Å) as compared to the V^{3+} ion (0.64 Å) to optimize the lattice strain, not all V^{3+} ions can accept charges from Ti^{3+} ions to form the correspondingly more stable V^{2+} ion. The $V^{3+}O_6$ and the much larger-sized $V^{2+}O_6$ octahedra [as shown in Figs. 4(d) and 4(e)] are accommodated by relative tiltings within the TiO_6 framework, which causes local Ti-O bond compressions along particular directions and, thus, helps in breaking the orbital degeneracy of the single electron of Ti^{3+} ions. To reduce the elastic-strain energy resulting from such a process, the compressions of the neighboring TiO_6 octahedra are mutually staggered among the three crystallographic directions (a, b and c) in the distorted cubic structure, causing the single electron occupation on the d_{yz}, d_{xz}, and d_{xy} Ti orbitals, respectively.

Figure 4(a) shows the DOS of the resultant insulating state. The DOS near the Fermi-level (E_F) as seen in Fig. 4(b) is primarily made up of V and Ti $3d$ levels with some small hybridization with O $2p$ orbitals. As seen in Fig. 4(b), which highlights the e_g and t_{2g} levels for various ionic valencies, the states across the band gap comprises primarily of t_{2g} levels of Ti^{3+} states (just below E_F) and the V^{3+} t_{2g} states (just above E_F). Expectedly, the V^{2+} levels, which are stabilized through the half-filled t_{2g} configuration, do not participate in the band-gap formation. The lowest-energy excitation of electrons in the presence of high-current flow, thus, occurs from Ti^{3+} to V^{3+} levels, leading to the lifting of orbital degeneracies of the electrons on both Ti and V ions and thereby melting of the JT-effect driven structural transition.

To summarize, we report breakdown of the Mott-insulating state in a spinel oxide system (MgTVO) at record-low threshold electric-field values. The Mott breakdown phenomenon seems to occur in MgTVO through an activated avalanche process following the Fröhlich two-temperature breakdown mechanism [51] (as suggested by Fig. 1(d) and some further checks as included in the Supplemental Material [28]). The in-gap electronic states, a crucial ingredient of the Fröhlich

model, likely has an intrinsic origin in MgTVO arising from partially excited Ti t_{2g} levels, however, further studies will be necessary to verify such a scenario. Importantly, however, the magnitude of the energy splitting in MgTVO is naturally a strong function of the cooperative JT lattice distortions (along with U) of the constituent V and Ti ions. In the presence of high-current flow, the transfer of electrons from Ti levels to V levels strongly affects the electronic configurations on these ions thereby modifying the JT distortions and, in turn, the gap value, triggering an avalanche process at a much smaller threshold electric-field value. In the event when the sample is cooled from a temperature above the structural transition temperature under the equilibrium condition or with a small current (such as 0.1- or 1-mA) flow, i.e., in the presence of negligible charge excitations, MgTVO undergoes a low-temperature cooperative JT-effect (arising from V^{3+} ions) driven structural transition from cubic (insulating) to the low-temperature tetragonal (insulating) phase. However, in a similar cooling run performed with high-current flow (above the threshold value, such as 100 mA) due to charge excitations from Ti towards V in the cubic phase, the resulting JT-inactive V^{2+} ions cannot drive anymore the cooperative JT-effect driven structural transition, and the sample continues to be in the metallic cubic phase (metallicity driven by charge excitations which facilitate charge transport involving vacant Ti^{4+} orbitals) until the lowest temperatures. This low-temperature cubic phase is, however, metastable, i.e., when the current flow is switched off at a lower temperature than the equilibrium structural transition temperature, reemergence of JT-active V^{3+} ions (along with Ti^{3+} ions) again leads to a cooperative JT-effect driven structural transition from the cubic phase into the tetragonal phase. Since the band gap of the tetragonal phase is relatively higher (because of associated JT distortions as seen in Fig. S14 of the Supplemental Material [28]), further current-induced tetragonal to cubic structural transition is not possible at the same temperature. A detailed thermal model analysis of experimental results on controlled nanodevices of MgTVO (likely to be the subject of a future study), would be helpful to further elucidate the driving mechanism for the resistive state transition in MgTVO.

We would like to acknowledge the DST-FIST measurement facility in the Department of Physics, IIT Kharagpur, India. D.C. would like to acknowledge SERB, DST, India (funding under Project File No. ECR/2016/000019) and BRNS, DAE (funding through Sanction No. 37(3)/20/23/2016-BRNS) for financial support. A.R. would like to acknowledge financial support from MHRD, India. A.R. and D.C. would also like to thank Dr. M. Chakraborty, Prof. P. Mahadevan, and Dr. S. Chatterjee for their help and fruitful discussions.

[1] E. Dagotto, Rev. Mod. Phys. **66**, 763 (1994).
[2] H. Hosono, A. Yamamoto, H. Hiramatsu, and Y. Ma, Mater. Today **21**, 278 (2018).
[3] D. Li, K. Lee, B. Y. Wang, M. Osada, S. Crossley, H. R. Lee, Y. Cui, Y. Hikita, and H. Y. Hwang, Nature (London) **572**, 624 (2019).
[4] S. Jin, T. H. Tiefel, M. McCormack, R. A. Fastnacht, R. Ramesh and L. H. Chen, Science **264**, 413 (1994).
[5] Y. Tokura and Y. Tomioka, J. Magn. Magn. Mater. **200**, 1 (1999).
[6] S. W. Cheong and M. Mostovoy, Nature Mater. **6**, 13 (2007).
[7] R. Ramesh and N. A. Spaldin, Nature Mater. **6**, 21 (2007).
[8] Y. Tokura and S. Seki, Adv. Mater. **22**, 1554 (2010).
[9] M. Imada, A. Fujimori, and Y. Tokura, Rev. Mod. Phys. **70**, 1039 (1998).
[10] P. Mahadevan, and D. D. Sarma, Phys. Rev. B **59**, 1739 (1999).
[11] Z. Liao, N. Gauquelin, R. J. Green, K. Müller-Caspary, I. Lobato, L. Li, S. V. Aert, J. Verbeeck, M. Hujiben, M. N. Grisolia, V. Rouco, R. El-Hage, J. E. Vilegas, A. Mercy, M. Bibes, P. Ghosez, G. A. Sawatzky, G. Rijnders, and G. Koster, Proc. Natl. Acad. Sci. USA **115**, 9515 (2018).
[12] K. Miyano, T. Tanaka, Y. Tomioka, and Y. Tokura, Phys. Rev. Lett. **78**, 4257 (1997).
[13] A. Asamitsu, Y. Tomioka, H. Kuwahara, and Y. Tokura, Nature (London) **388**, 50 (1997).
[14] S. Yamanouchi, Y. Taguchi, and Y. Tokura, Phys. Rev. Lett. **83**, 5555 (1999).
[15] Y. Taguchi, T. Matsumoto, and Y. Tokura, Phys. Rev. B **62**, 7015 (2000).
[16] P. Stoliar, L. Cario, E. Janod, B. Corraze, C. Guillot-Deudon, S. Salmon-Bourmand, V. Guiot, J. Tranchant, and M. Rozenberg, Adv. Mater. **25**, 3222 (2013).
[17] P. Diener, E. Janod, B. Corraze, M. Querré, C. Adda, M. Guilloux-Viry, S. Cordier, A. Camjayi, M. Rozenberg, M. P. Besland, and L. Cario, Phys. Rev. Lett **121**, 016601 (2018).
[18] C. Sow, S. Yonejawa, S. Kitamura, T. Oka, K. Kuroki, F. Nakamura, and Y. Maeno, Science **358**, 1084 (2017).
[19] J. Bertinshaw, N. Gurung, P. Jorba, H. Liu, M. Schmid, D. T. Mantadakis, M. Daghofer, M. Krautloher, A. Jain, G. H. Ryu, O. Fabelo, P. Hansmann, G. Khaliullin, C. Pfleiderer, B. Keimer, and B. J. Kim, Phys. Rev. Lett. **123**, 137204 (2019).
[20] M. Schmidt, W. Ratcliff, II, P. G. Radaelli, K. Refson, N. M. Harrison, and S. W. Cheong, Phys. Rev. Lett. **92**, 056402 (2004).
[21] M. Isobe and Y. Ueda, J. Phys. Soc. Jpn. **71**, 1848 (2002).
[22] S. Leoni, A. N. Yaresko, N. Perkins, H. Rosner, and L. Craco, Phys. Rev. B **78**, 125105 (2008).
[23] D. I. Khomskii and T. Mizokawa, Phys. Rev. Lett. **94**, 156402 (2005).
[24] S. Di Matteo, G. Jackeli, C. Lacroix, and N. B. Perkins, Phys. Rev. Lett. **93**, 077208 (2004).
[25] S. Niitaka, H. Ohsumi, K. Sugimoto, S. Lee, Y. Oshima, K. Kato, D. Hashizume, T. Arima, M. Takata, and H. Takagi, Phys. Rev. Lett. **111**, 267201 (2013).
[26] G. Mazza, A. Amaricci, M. Capone, and M. Fabrizio, Phys. Rev. Lett. **117**, 176401 (2016).
[27] T. Roisnel and J. Rodŕlguez-Carvajal, *Epdic 7: Proceedings of the Seventh European Powder Diffraction Conference, Barcelona, Spain, 2000*, Materials Science Forum, edited by R. Delhez and E. J. Mittemeijer (Trans Tech Publications Inc., Barcelona, Spain, 2000), Vols. 378–381, pp. 118–123.
[28] Supplemental Material at http://link.aps.org/supplemental/10.1103/PhysRevB.103.245145 contains supporting electrical and

structural data. Comparative DOS and discussion on the Fröhlich model are also included.

[29] J. W. Borchert, B. Peng, F. Letzkus, J. N. Burghartz, P. K. L. Chan, K. Zojer, S. Ludwigs, and H. Klauk, Nat. Commun. **10**, 1119 (2019).

[30] M. Devika, N. K. Reddy, F. Patolsky, and K. R. Gunasekhar, J. Appl. Phys. **104**, 124503 (2008).

[31] G. Kresse, and J. Hafner, Phys. Rev. B **47**, 558 (1993); **48**, 13115 (1993); **49**, 14251 (1994).

[32] S. L. Dudarev, G. A. Botton, S. Y. Savrasov, C. J. Humphreys, and A. P. Sutton, Phys. Rev. B **57**, 1505 (1998).

[33] S. Bose, R. Banerjee, A. Genc, P. Raychaudhuri, H. L. Fraser, and P. Ayyub, J. Phys.: Condens. Mater. **18**, 4553 (2006).

[34] W. Sugimoto, H. Yamamoto, Y. Sugahara, and K. Kuroda, J. Phys. Chem. Solids **59**, 83 (1998).

[35] D. B. Rogers, J. L. Grillson, and T. E. Gier, Solid State Commun. **5**, 263 (1967).

[36] I. Valmianski, P. Y. Wang, S. Wang, J. G. Ramirez, S. Guenon, and I. K. Schuller, Phys. Rev. B **98**, 195144 (2018).

[37] G Stefanovich, A Pergament, and D Stefanovich, J. Phys.: Condens. Mater. **12**, 8837 (2000).

[38] G. Gopalakrishnan, D. Ruzmetov, and S. Ramanathan, J. Mater. Sci **44**, 5345 (2009).

[39] P. Stoliar, M. Rozenberg, E. Janod, B. Corraze, J. Tranchant, and L. Cario, Phys. Rev. B **90**, 045146 (2014).

[40] Y. Kalcheim, A. Camjayi, J. d. Valle, P. Salev, M. Rozenberg, and I. K. Schuller, Nat. Commun. **11**, 2985 (2020).

[41] S. Lee, A. Fursina, J. T. Mayo, C. T. Yavuj, V. L. Colvin, R. J. S. Sofin, I. V. Shvets, and D. Natelson, Nature Mater. **7**, 130 (2008).

[42] A. A. Fursina, R. G. S. Sofin, I. V. Shvets, and D. Natelson, Phys. Rev. B **79**, 245131 (2009).

[43] E. C. dos Santos, D. C. Freitas, I. Fier, J. C. Fernandes, M. A. Continentino, A. J. A de Oliveira, and L. Walmsley, J. Phys. Chem. Solids **90**, 65 (2016).

[44] C. Cirillo, V. Granata, G. Avallone, R. Fittipaldi, C. Attanasio, A. Avella, and A. Vecchione, Phys. Rev. B **100**, 235142 (2019).

[45] V. Guiot, L. Cario, E. Janod, B. Corraze, V. Ta Phuoc, M. Rozenberg, P. Stoliar, T. Cren, and D. Rodhitchev, Nat. Commun. **4**, 1722 (2013).

[46] H. D. Zhou and J. B. Goodenough, Phys. Rev. B. **72**, 045118 (2005).

[47] E. Hryha, E. Rutqvist, and L. Nyborg, Surf. Interface. Anal **44**, 1022 (2011).

[48] A. Rahaman, M. Chakraborty, T. Paramanik, R. K. Maurya, S. Mahana, R. Bindu, D. Topwal, P. Mahadevan, and D. Choudhury, Phys. Rev. B **100**, 115162 (2019).

[49] T. Sonehara, K. Kato, K. Osaka, M. Takata, and T. Katsufuji, Phys. Rev. B **74**, 104424 (2006).

[50] S. K. Pandey, Phys. Rev. B **84**, 094407 (2011).

[51] H. Frohlich, Proc. R. Soc. A **188**, 521 (1947).